Journal of Power Sources 238 (2013) 350–355

Contents lists available at SciVerse ScienceDirect

Journal of Power Sources

journal homepage: www.elsevier.com/locate/jpowsour

Vertically aligned anatase TiO_2 nanowire bundle arrays: Use as Pt support for counter electrodes in dye-sensitized solar cells

Guohui Tian [a,b], Kai Pan [a], Yajie Chen [a], Juan Zhou [a], Xiaohuan Miao [a], Wei Zhou [a], Ruihong Wang [a], Honggang Fu [a,*]

[a] Key Laboratory of Functional Inorganic Material Chemistry, Ministry of Education of the People's Republic of China, Heilongjiang University, Harbin 150080, PR China

[b] Key Laboratory of Chemical Engineering Process & Technology for High-efficiency Conversion, College of Heilongjiang Province, School of Chemistry and Materials Science, Heilongjiang University, Harbin 150080, PR China

HIGHLIGHTS

- Vertically anatase TiO_2 nanowire bundle array is prepared.
- The TiO_2 nanowire array is used as Pt support to fabricate counter electrode.
- The counter electrode provides more active sites and higher charge transfer.
- An enhanced conversion efficiency was obtained.

GRAPHICAL ABSTRACT

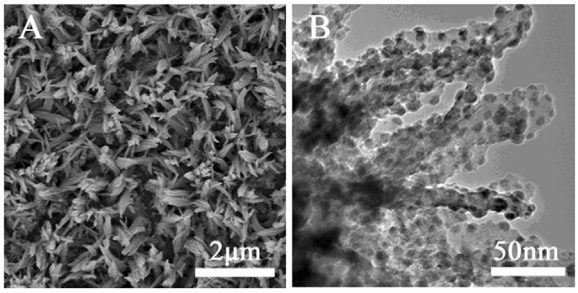

ARTICLE INFO

Article history:
Received 4 February 2013
Received in revised form
15 March 2013
Accepted 25 March 2013
Available online 11 April 2013

Keywords:
Anatase titania nanowire bundle array
Counter electrode
Dye-sensitized solar cell
Catalytically active sites

ABSTRACT

Vertically aligned anatase TiO_2 nanowire bundle arrays are prepared via a solvothermal and subsequent calcination process. Pt nanoparticles with a size of 4–6 nm are uniformly immobilized on TiO_2 nanowire bundle array to obtain Pt/TiO_2 nanowire bundle array counter electrode, which can remarkably enhance catalytically active sites and provide facile transport of ions and electrons. The as-prepared materials are characterized by scanning electron microscopy, transmission electron microscopy and X-ray diffraction. The dye-sensitized solar cell (DSSC) fabricated with Pt/TiO_2 nanowire bundle array counter electrode shows significantly higher photovoltaic performance than the conventional Pt counter electrode.

1. Introduction

TiO_2 is an important semiconductor material that is used in the fields of photocatalysis and dye-sensitized solar cells (DSSCs) [1,2]. The performance of the TiO_2 is strongly dependent on its phase structure, morphology and other properties [3–5]. Recent studies have suggested that one dimensional (1D) TiO_2 nanomaterials such as nanowires and nanotubes, offering direct pathways for photogenerated electrons transfer, possesses advantages such as facile charge transport along the longitudinal dimension and low electron–hole recombination rate [6–9]. Therefore, 1D TiO_2 has attracted extensive attention as a substitute for randomly oriented titania nanoparticles, and manifested superior photovoltaic and superhydrophilicity performance [10–12]. Research progress nowadays has further showed that 1D nanostructures can be assembled into nanofibrous membranes to improve the photovoltage performance

* Corresponding author. Tel.: +86 451 8660 4330; fax: +86 451 8667 3647.
E-mail address: fuhg@vip.sina.com (H. Fu).

0378-7753/$ – see front matter © 2013 Elsevier B.V. All rights reserved.
http://dx.doi.org/10.1016/j.jpowsour.2013.03.184

and self-cleaning ability [13]. However, compared with the disordered 1D nanostructures used as photoanodes, an array of highly ordered, vertically aligned 1D nanostructures have exhibited more excellent performance of the DSSCs because the aligned nanostructure perpendicular to the substrate could potentially improve the charge-collection efficiency [14–17]. However, as far as we know, the vertically aligned 1D anatase TiO_2 has not been exploited to be used as Pt support to prepare the counter electrodes of DSSCs.

The counter electrode for DSSCs is required to have both high conductivity and excellent catalytic properties [18–22]. It is not easy, however, to simultaneously satisfy both requirements. The counter electrode of DSSCs usually utilizes a thin Pt film on a conducting glass substrate. Although many other materials such as carbon [23], conductive polymer [24], and some inorganic compounds have been introduced as inexpensive alternatives [25–28], Pt is still the cornerstone material because of its highly catalytic activity and superior chemical and electrochemical stability [29–31]. Recently, to lower the cost and meanwhile improve the mechanical rigidity and stability of the electrocatalyst, such as bilayer Pt/Nd-doped mesoporous TiO_2 and Pt/TiO_2 nanoparticles films have been prepared and showed enhanced overall energy conversion efficiency compared to the conventional Pt counter electrode [32–34]. However, to the best knowledge of the authors, the vertically aligned 1D anatase TiO_2 has not been exploited to be used as Pt support to prepare the counter electrodes of DSSCs. Recently, one-dimension composite counter electrodes have been proved to have the synergistic effect for I_3^- reduction and showed excellent electrocatalytic activity for I_3^- reduction [35,36]. Because the vertically aligned 1D architecture can offer more active sites and direct electron transfer pathways compared with the flat solid nanoparticles film, so Pt/1D TiO_2 counter electrode may provide better energy conversion efficiency.

In the present work, vertically aligned TiO_2 nanowire bundle array was prepared and used as Pt support to fabricate counter electrode for the first time. The material structure, catalytic activity toward triiodide reduction, and the photovoltaic responses of device incorporated with this counter electrode were investigated. Interestingly, as the result of numerous catalytically active sites and the facile transport of ions and electrons, the obtained Pt/TiO_2 nanowire bundle array counter electrode exhibited superior electrocatalytic activity toward triiodide reduction compared with that of the conventional sputtered Pt counter electrode.

2. Experimental

2.1. Synthesis of vertically aligned anatase TiO_2 nanowire bundle array

In a typical case, 0.5 ml titanium isopropoxide (TTIP) and 4 ml glycerol were successively added in 20 ml of ethanol under ultrasonic. The resulting mixed solution was transferred into a 50 ml Teflon-lined stainless steel autoclave. Then the thoroughly cleaned FTO conductive glass substrates were immersed in the solution in a certain angle. The teflon-lined stainless steel autoclave containing mixture solution was then heated to 170 °C and maintained for 8 h. Subsequently, the autoclave was cooled to room temperature naturally. The as-obtained films were rinsed with ethanol, dried at 70 °C and then annealed at 450 °C in air for 2 h.

2.2. Fabrication of Pt/TiO_2 counter electrodes

The Pt/TiO_2 (Pt/TiO_2 nanowire bundle array and Pt/TiO_2 nanoparticle) counter electrodes were prepared by an ion sputtering coater (SBC-12, KYKY Technology Development Ltd., China) with duration of 120 s. For comparison, a Pt electrode was also obtained using the same sputtering time.

2.3. Fabrication of DSSCs

TiO_2 working photoanodes about ~12 μm were prepared on FTO substrate using TiO_2 (P25) paste by doctor blade technique and subsequently sintered at 450 °C for 30 min in ambient atmosphere. The sensitization of the photoelectrodes was achieved by immersing them into 0.5 mM cis-bis (isothiocyanato) bis (2,2′-bipyridyl-4,4′-dicarboxylato) ruthenium (II) bistetrabutylammonium (N719, Solaronix SA, Switzerland) dye solution for 48 h. The dye-sensitized TiO_2 photoanodes and the prepared counter electrodes were adhered together with epoxy resin, respectively. The space between the two electrodes was filled with the redox shuttle electrolyte by capillary action. The redox shuttle electrolyte was composed of 0.1 M LiI (anhydrous, 99%, Acros), 0.05 M I_2 (≥99.8%), 0.5 M tert-butylpyridine (99%, Aldrich) and 0.6 M 1-propyl-2, 3-dimethylimidazolium iodide (99%) in acetonitrile (99%, Fluka). The fabricated DSSCs based on Pt/TiO_2 nanowire bundle array, Pt/TiO_2 nanoparticle and Pt counter electrodes were labeled as C1, C2 and C3, respectively.

2.4. Materials characterization

The structure and morphology of the product was investigated by FE-SEM (Hitachi S-4800, Japan), TEM (JEOL 2100, Japan) and powder XRD (diffractometer D/max 2500 using CuKa radiation). Photovoltaic measurements were carried out with a solar simulator (Oriel, USA) equipped with an AM1.5G filter (Oriel, USA). The power of the simulated light was calibrated to 100 mW cm^{-2} by using an Oriel Solar Simulator radio meter. Photocurrent–photovoltage curves were obtained by applying an external photo-mask of 0.12 cm^2 and measuring the generated photocurrent with a BAS100B electrochemical analyzer (Bioanalytical Systems Inc., USA). In a standard three-compartment cell, the prepared Pt/TiO_2, Pt and a saturated calomel electrode (SCE) were used as the working electrode, counter electrode and reference electrode, respectively. The electrolyte was acetonitrile containing 0.1 M $LiClO_4$ as the supporting electrolyte, 10 mM LiI and 1 mM I_2 as the redox couple, scan rate is 10 mV s^{-1}. The EIS were performed with a computer-controlled IM6e impedance measurement unit (Zahner Elektrik, Germany) and carried out by applying sinusoidal perturbations of 10 mV under bias of −0.8 V, and the frequency ranges from 0.05 to 100 kHz. The obtained spectra were fitted with ZsimpWin software in terms of appropriate equivalent circuits.

3. Results and discussion

3.1. Characterization of the TiO_2 nanowire bundle arrays

The as-synthesized anatase TiO_2 nanowire bundle arrays were characterized by SEM and TEM. The top and cross-sectional view SEM images of the anatase TiO_2 nanowire bundle arrays in Fig. 1A and B show that there are many vertically aligned nanowire bundles. Each nanowire in these bundles is composed of nanoparticles with uniform diameters of 8–12 nm, which can be seen from TEM images (Fig. 1C). The selected area electron diffraction (SAED) patterns (inset of Fig. 1C) and HRTEM image in Fig. 1D (the magnification of the white square part in Fig. 1C) reveal that the TiO_2 nanowire bundles show polycrystalline phases of anatase TiO_2 with a (101) interplanar space of 0.352 nm. The XRD pattern (line d) in Fig. 2B also shows a series of broad diffraction peaks which correspond to the anatase structure (JCPDS #21-1272). However, the XRD pattern (line d) in Fig. 2A of the precursor film exists several sharp peaks at low angle region (10–13°) with several weak ones at high low angle region, which is similar to that of the reported metal glycerolate complexes, indicating the formation of titanium glycerolate precursor [37,38]. SEM image (Fig. 3D) of the

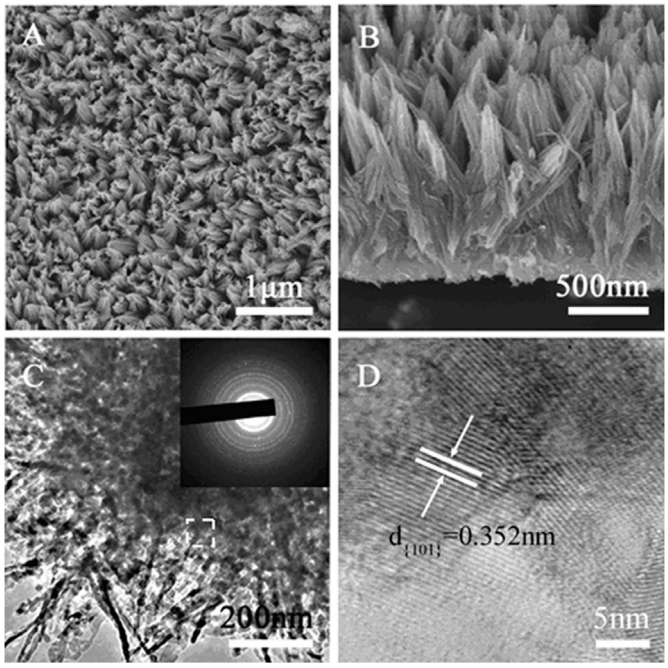

Fig. 1. SEM images of the top surface (A) and edge surface (B) of the TiO_2 nanowire bundle arrays; TEM (C) and HRTEM (D) images of the TiO_2 nanowire bundle arrays.

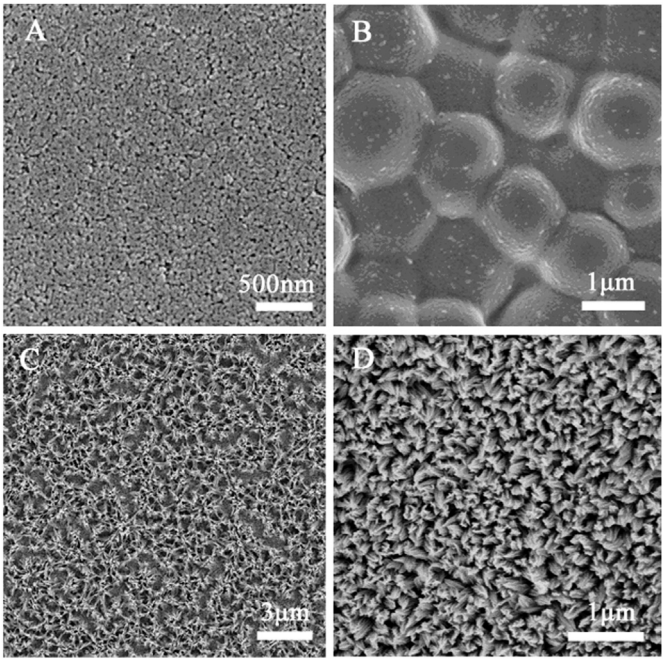

Fig. 3. SEM images showing the morphological evolution of the obtained precursor films prepared from different reaction time: (A) 10 min; (B) 0.5 h; (C) 2 h; (D) 8 h.

precursor also shows the nanowire bundle array structure. It indicated that calcination did not change the integral appearance of the nanowire bundle array structure.

In order to elucidate the growth process of nanowire bundle array precursor, the experiments were carried out under various reaction intervals. SEM images in Fig. 3 showed the morphology changes of the precursors obtained from different reaction time. The SEM surface morphological image A in Fig. 3 clearly revealed that the surface of the film is made up of small nanoparticles (20–30 nm) with relative uniformity after 10 min reaction. Nanoparticles are amorphous titanium oxyhydrate nanoparticles, which can be seen from the XRD pattern (Line a, Fig. 2A). With further increasing reaction time to 0.5 h, the formed nanoparticles further aggregated and grew into microspheres predominantly 300–450 nm in diameter. When the reaction time is 3 h, the surface morphology of the film has an obvious change, small 1D nanowires (Fig. 3C) formed on the surface of the microsphere film perpendicular to the FTO substrate. With further extending the reaction time, long nanowire bundle array (Fig. 3D) is finally formed.

Based on the above experimental results, the formation of the nanowire bundle array precursor could be interpreted in terms of fast nucleation and nuclei aggregate, dissolution–recrystallization and confined growth process (Fig. 4). In this formation process, amorphous titanium oxyhydrate nanoparticles film formed from the fast hydrolysis and alcoholysis reactions of the titanium isopropoxide. Then the formed nanoparticle further aggregated and grew into microspheres driven by reducing the surface energy of nanoparticles. With the extension of reaction time, the formed amorphous titanium oxyhydrate on the surface of the microsphere films gradually reacted with glycerol and form titanium glycerolate complexes, as can be confirmed from XRD (line c, d in Fig. 2A). Similar to the previous report that the reaction between polyalcohol with metal ion usually form 1D coordination complexes, in this experiment, small 1D nanowires formed perpendicular to the FTO substrate due to the confinement effect of the FTO glass [39], and long nanowire bundle array (Fig. 3D) finally formed via the further growth. All the precursor complexes transformed into anatase TiO_2 without changing the integral nanowire bundle array morphology after calcination.

3.2. Characterization of the Pt/TiO_2 nanowire bundle array

The detailed morphology and microstructure of TiO_2 nanowire bundle array after Pt sputtering were also characterized by SEM and TEM. As shown in Fig. 5C, D, Pt nanoparticles with a diameter of 4–6 nm are uniformly deposited on the surface of TiO_2 nanowires. It

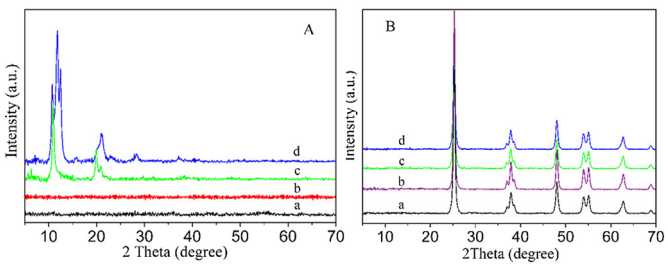

Fig. 2. XRD patterns of the precursors (A) prepared from different reaction time: (a) 10 min, (b) 0.5 h, (c) 2 h and (d) 8 h and corresponding products after calcination (B).

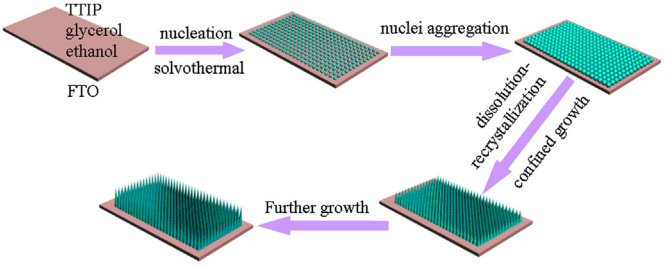

Fig. 4. Schematic diagram of the formation process of nanowire bundle array precursor on FTO substrate.

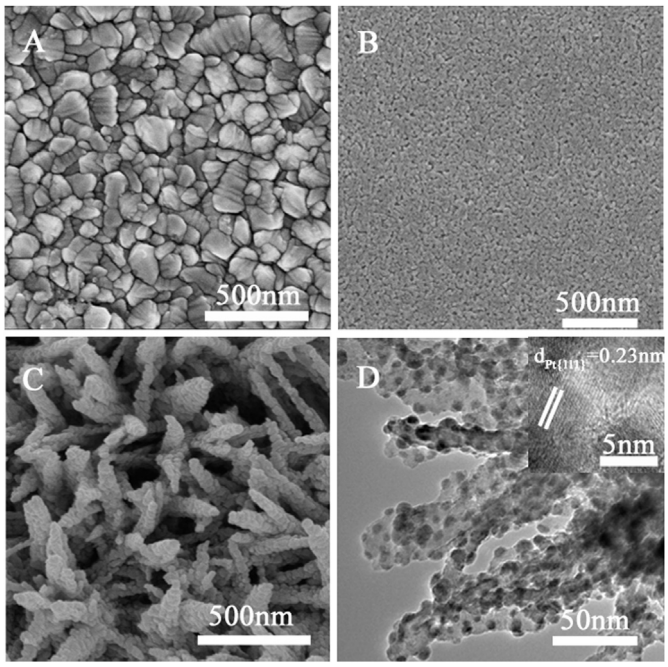

Fig. 5. SEM images of Pt/FTO film (A), Pt/TiO_2 nanoparticle film (B) and Pt/TiO_2 nanowire bundle array (C); (HR)TEM (D) image of Pt/TiO_2 nanowire bundle array.

indicates that TiO_2 nanowires can provide numerous sites to deposit well-dispersed Pt nanoparticles avoiding excess aggregation. In contrast, Pt nanoparticles sputtered on the surfaces of FTO glass (Fig. 5A) and TiO_2 nanoparticle film (Fig. 5B) aggregated into relatively flat nanoparticle film.

3.3. Analysis of the electrochemical properties of the different counter electrodes

Subsequently, the DSSCs of C1, C2 and C3 were fabricated using Pt/TiO_2 nanowire array bundle array, Pt/TiO_2 nanoparticle and Pt as counter electrodes, respectively, as described in the experimental section. The catalytic performances of the counter electrodes were independently analyzed by cyclic voltammetry (CV) measurements. As indicated in Fig. 6, the relative negative pair is assigned to the oxidation and reduction of I^-/I_3^-, whereas the positive pair is assigned to the oxidation and reduction of I_2/I_3^- [40]. In Fig. 6, the Pt/TiO_2 nanowire bundle array-based counter electrode shows a much larger current density for the I_3^- reduction and I^- oxidation than both of the conventional Pt and Pt/TiO_2 nanoparticle film-based

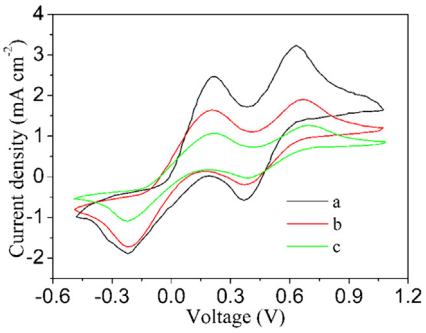

Fig. 6. Cyclic voltammograms of Pt/TiO_2 nanowire bundle array (a), Pt/TiO_2 nanoparticle (b) and Pt (c) electrodes using an acetonitrile solution containing 0.1 M $LiClO_4$, 0.01 M lil and 0.001 M I_2 as the supporting electrolyte, scan rate = 10 mV s^{-1}.

counter electrodes, which means a faster redox reaction rate and a better electrocatalytic activity for the I^-/I_3^- redox couple on the Pt/TiO_2 nanowire bundle array-based counter electrode. The highest apparent catalytic activity of Pt/TiO_2 nanowire bundle array observed in CV measurement is attributed to its most effective catalytic active sites. Because of its 1D vertical structure, the 1D TiO_2 nanowire bundle array possesses largest effective surface area compared to the flat Pt nanoparticle and TiO_2 nanoparticle film. Therefore, it can hold more Pt nanoparticles uniformly dispersed on the surface, and therefore can provide more catalytic active sites for the reduction of I_3^- and direct electron transport pathways than the flat Pt and Pt/TiO_2 nanoparticle film-based counter electrodes (Fig. 5A and B). Moreover, the Pt/TiO_2 nanowires are interconnected and porous, which are more favorable for the electrolyte permeation, contributing to the improvement of electrocatalytic activity.

Table 1 summarizes the photovoltaic parameters obtained from photocurrent density–voltage (J–V) curves (Fig. 7) of DSSCs with three different counter electrodes. The C1 fabricated with Pt/TiO_2 nanowire bundle array counter electrode showed a conversion efficiency of about 6.50%, which is 9.7% higher than that of the C2 based on the Pt/TiO_2 nanoparticle counter electrode (5.92%), respectively. The C3 fabricated with Pt counter electrode, however, achieved a conversion efficiency of 5.24%, much lower (24%) than that of the Pt/TiO_2 nanowire bundle array, mainly due to a lower fill factor of 0.59. It was apparent that the enhancement of the η was directly originated from the FF increase. Because the FF is attenuated by the total series resistance of the cell, the FF enrichment in this work can be mainly profited from the superior electrocatalytic activity of the Pt/TiO_2 nanowire bundle array counter electrode and consequent significantly reduced charge transfer resistance (R_{ct}) across the counter electrode/electrolyte interface [41]. Furthermore, the higher photocurrent density of the Pt/TiO_2 nanowire bundle array counter electrode (J_{sc} = 14.29 mA cm^{-2}) with respect to that of the Pt counter electrode (J_{sc} = 12.70 mA cm^{-2}) may arise from the efficient reduction reaction in the I^-/I_3^- system because of its increased active area, as was discussed in the cyclic voltammetry analysis. The overall characteristics of the Pt/TiO_2 nanowire bundle array composite counter electrode reveal its reliable performance comparable with that of Pt/TiO_2 nanoparticle and conventional Pt counter electrodes.

To interpret the role of the three fabricated counter electrodes in the DSSCs system, electrochemical impedance spectroscopy (EIS) measurements were carried out to compare the charge transfer and ion transport characteristics of the different electrodes. Nyquist plots for the different materials are shown in Fig. 8. The circuit model used to fit the experimental EIS data is shown in the inset of Fig. 8. The EIS data in this work are helpful for understanding all of the composite nanostructure solar cells, and can also explain well the existing interfaces in DSSCs. Many theoretical models were proposed to interpret the complex system of the DSSC under different conditions. The equivalent model fitting the impedance spectra of C1, C2 and C3 is shown in inset of Fig. 8. The symbols of R and C represent a resistance and a capacitance, respectively. C_1 is the charge-transfer resistance and double-layer capacitance at the counter electrode, respectively. C_2 is the chemical capacitance of the photoelectrode film that accounts for the change of electron density as a function of the Fermi level. R_s is a series resistance standing for

Table 1
Photovoltaic properties of the DSSCs fabricated with different counter electrodes.

Cells	J_{sc}/mA cm^{-2}	V_{OC}/V	FF	η/%
C1	14.29	0.699	0.76	6.50
C2	12.94	0.667	0.68	5.92
C3	12.70	0.689	0.59	5.24

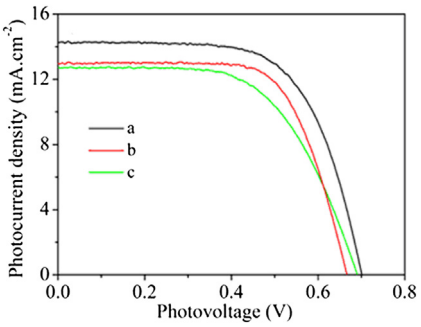

Fig. 7. Photocurrent–voltage curves of different DSSCs fabricated with different counter electrodes: C1 (a) based on Pt/TiO_2 nanowire bundle array, C2 (b) based on Pt/TiO_2 nanoparticle and C3 (c) based on Pt counter electrodes.

the transport resistance of the two FTO electrodes. R_{ct1} is the electrocatalytic resistance at the interface between the electrolyte and the counter electrode, R_{ct2} is the charge-transfer resistance at the interface of TiO_2/dye/electrolyte, and Z_{Dif} represents the Warburg impedance of I^-/I_3^- in the electrolyte. Where the impedance of the finite-length Warburg diffusion can be expressed by

$$Z_{Dif} = R_{Dif}\left\{\left[\tanh(j\omega\tau)^{1/2}\right]/(j\omega\tau)^{1/2}\right\} \quad (1)$$

where $R_{Dif} = B/Y_{O1}$, $\tau = B^2$, B was parameter [42]. The EIS data obtained by fitting the impedance spectra of C1, C2 and C3 using the equivalent model of Fig. 8 are shown in Table 2. The EIS data in this work are helpful for understanding of all composite nanostructure solar cells, and also can explain well the existing interfaces in DSSCs. It can be clearly seen that R_{ct1}, is 0.61 Ω for C1, 0.78 Ω for C2 and 1.05 Ω for C3. A lower interface resistance will result in faster interfacial electron transfer. This order confirms the results of the I–V curves of these DSSCs. Amongst them, the C1 cell based on the Pt/TiO_2 nanowire bundle array-based electrode displays the fastest electron transfer rate, and thus the highest η. The reduced resistance can be attributed to the enhanced charge transfer between the Pt/TiO_2 nanowire bundle array-based counter electrode and the electrolyte. It demonstrates that the transport of charge carriers along the TiO_2 nanowire bundle array is more facile than the random particles. The EIS data obtained by fitting the impedance spectra show that Warburg impedance (Z_{Dif}) of the Pt/TiO_2 nanowire bundle array composite electrode (45.4 Ω) was lesser than the Pt/TiO_2 nanoparticle (54.5 Ω) and conventional Pt (65.6 Ω) counter electrodes. It is mainly because that the Pt/TiO_2 nanowire bundle

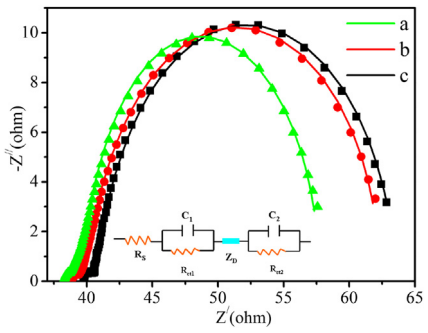

Fig. 8. Nyquist plots of measured EIS spectra of different DSSCs fabricated with different counter electrodes: C1 (a) based on Pt/TiO_2 nanowire bundle array, C2 (b) based on Pt/TiO_2 nanoparticles and C3 (c) based on Pt. The insets show the equivalent circuit of the device.

Table 2
Parameters determined by EIS measurements.

Cells	R_s/Ω	R_{ct1}/Ω	C_1/F	Z_{Dif}		R_{ct2}/Ω	C_2/F
				Y_0/S	B/S$^{1/2}$		
C1	38.54	0.61	7.2E-5	2.4E-2	0.35	21.82	1.72E-4
C2	39.07	0.78	4.6E-5	2.8E-2	0.33	21.56	2.69E-4
C3	39.85	1.05	2.8E-5	3.6E-2	0.29	21.45	2.24E-4

array counter electrode possesses porous structure between the TiO_2 nanowires, in which ionic diffusion is favorable with small hindrance. In contrast, Pt/TiO_2 nanoparticle and conventional Pt counter electrodes possess flat solid surface, which are not beneficial to the ionic diffusion [43].

4. Conclusions

In summary, we synthesized the vertically aligned anatase TiO_2 nanowire bundle array through a simple solvothermal and subsequent calcination. Pt nanoparticles with a size of 4–6 nm were uniformly immobilized on TiO_2 nanowire bundle array to obtain Pt/TiO_2 nanowire bundle array counter electrode. The DSSCs fabricated with the Pt/TiO_2 nanowire bundle array counter electrode showed significantly higher efficiency than that using the conventional Pt counter electrode. The enhanced performance can be mainly attributed to the fact that the obtained Pt/TiO_2 nanowire bundle array counter electrode can provide more catalytically active sites and facile transport of ions and electrons.

Acknowledgments

This research was supported by the National Natural Science Foundation of China (51272070, 21031001, 21001042, 21101060, 21201058), the Cultivation Fund of the Key Scientific and Technical Innovation Project, Ministry of Education of China (No 708029), Research Fund for the Doctoral Program of Higher Education of China (20112301110002).

References

[1] H.B. Wu, H.H. Hng, X.W. Lou, Adv. Mater. 24 (2012) 2567–2571.
[2] B. O'Regan, M. Grätzel, Nature 353 (1991) 737–740.
[3] W.X. Guo, C. Xu, X. Wang, S.H. Wang, C.F. Pan, C.J. Lin, Z.L. Wang, J. Am. Chem. Soc. 134 (2012) 4437–4441.
[4] G.H. Tian, Y.J. Chen, H.L. Bao, X.Y. Meng, K. Pan, W. Zhou, C.G. Tian, J.Q. Wang, H.G. Fu, J. Mater. Chem. 22 (2012) 2081–2088.
[5] M. Es-Souni, M. Es-Souni, S. Habouti, N. Pfeiffer, A. Lahmar, M. Dietze, C.-H. Solterbeck, Adv. Funct. Mater. 20 (2010) 377–385.
[6] M. Law, L.E. Greene, J.C. Johnson, R. Saykally, P.D. Yang, Nat. Mater. 4 (2005) 455–459.
[7] E. Galoppini, J. Rochford, H.H. Chen, G. Saraf, Y.C. Lu, A. Hagfeldt, G. Boschloo, J. Phys. Chem. B 110 (2006) 16159–16161.
[8] D.J. Yang, H.W. Liu, Z.F. Zheng, Y. Yuan, J.-C. Zhao, E.R. Waclawik, X.B. Ke, H.Y. Zhu, J. Am. Chem. Soc. 131 (2009) 17885–17893.
[9] D. Kim, A. Ghicov, S.P. Albu, P. Schmuki, J. Am. Chem. Soc. 130 (2008) 16454–16455.
[10] P.A. Sedach, T.J. Gordon, S.Y. Sayed, T. Furstenhaupt, R.H. Sui, T. Baumgartner, C.P. Berlinguette, J. Mater. Chem. 20 (2010) 5063–5069.
[11] A.B.F. Martinson, J.E. McGarrah, M.O.K. Parpia, J.T. Hupp, Phys. Chem. Chem. Phys. 8 (2006) 4655–4659.
[12] X.J. Feng, K. Shankar, O.K. Varghese, M. Paulose, T.J. Latempa, C.A. Grimes, Nano Lett. 8 (2008) 3781–3786.
[13] P. Sudhagar, V. Gonzalez-Pedro, I. Mora-Sero, F. Fabregat-Santiago, J. Bisquert, Y.S. Kang, J. Mater. Chem. 22 (2012) 14228–14235.
[14] B. Liu, A. Khare, E.S. Aydil, Chem. Commun. 48 (2012) 8565–8567.
[15] B. Liu, E.S. Aydil, J. Am. Chem. Soc. 131 (2009) 3985–3990.
[16] S.C. Hou, X. Cai, H.W. Wu, Z.B. Lv, D. Wang, Y.P. Fu, D.C. Zou, J. Power Sources 215 (2012) 164–169.
[17] K. Zhu, N.R. Neale, A. Miedaner, A.J. Frank, Nano Lett. 7 (2007) 69–74.
[18] X.W. Zeng, W.J. Zhang, Y. Xie, D.H. Xiong, W. Chen, X.B. Xu, M.K. Wang, Y.-B. Cheng, J. Power Sources 226 (2013) 359–362.

[19] S.J. Peng, J. Liang, S.G. Mhaisalkar, S. Ramakrishna, J. Mater. Chem. 22 (2012) 5308–5311.
[20] C.G. Bu, Q.D. Tai, Y.M. Liu, S.S. Guo, X.Z. Zhao, J. Power Sources 221 (2013) 78–83.
[21] J.S. Jang, D.J. Ham, E. Ramasamy, J. Lee, J.S. Lee, Chem. Commun. 46 (2010) 8600–8602.
[22] X. Yin, Z.S. Xue, B. Liu, J. Power Sources 196 (2011) 2422–2426.
[23] K.S. Lee, W.J. Lee, N.G. Park, S.O. Kim, J.H. Park, Chem. Commun. 47 (2011) 4264–4266.
[24] T.L. Hsieh, H.W. Chen, C.W. Kung, C.C. Wang, R. Vittala, K.C. Ho, J. Mater. Chem. 22 (2012) 5550–5559.
[25] Q.W. Jiang, G.R. Li, X.P. Gao, Chem. Commun. (2009) 6720–6722.
[26] M.k. Wang, A.M. Anghel, B. Marsan, N.-L. Cevey Ha, N. Pootrakulchote, S.M. Zakeeruddin, M. Grätzel, J. Am. Chem. Soc. 131 (2009) 15976–15977.
[27] J.Y. Lin, J.H. Liao, S.W. Chou, Electrochim. Acta 56 (2011) 8818–8826.
[28] H. Sun, D. Qin, S. Huang, X. Guo, D. Li, Y. Luo, Q. Meng, Energy Environ. Sci. 4 (2011) 2630–2637.
[29] K. Seok Lee, H.K. Lee, D.H. Wang, N.G. Park, J.Y. Lee, O.O. Park, J.H. Park, Chem. Commun. 46 (2010) 4505–4507.
[30] S. Soo Jeon, C. Kim, J.J. Ko, S.S. Im, J. Mater. Chem. 21 (2011) 8146–8151.
[31] M.X. Wu, X. Lin, A. Hagfeldtb, T.L. Ma, Chem. Commun. 47 (2011) 4535–4537.
[32] P. Hasin, M.A. Alpuche-Aviles, Y.G. Li, Y.Y. Wu, J. Phys. Chem. C 113 (2009) 7456–7460.
[33] S.S. Kim, K.W. Park, J.H. Yum, Y.E. Sung, J. Photochem. Photobiol. A 189 (2007) 301–306.
[34] F. Hao, H. Lin, Y.Z. Liu, N. Wang, W.D. Li, J.B. Li, ACS Appl. Mater. Interfaces 3 (2011) 3916–3920.
[35] S.-Y. Tai, C.-J. Liu, S.-W. Chou, F.S.-S. Chien, J.-Y. Lin, T.-W. Lin, J. Mater. Chem. 22 (2012) 24753.
[36] G.-R. Li, F. Wang, Q.-W. Jiang, X.-P. Gao, P.-W. Shen, Angew. Chem. Int. Ed. 49 (2010) 3653.
[37] C.Q. Wang, D.R. Chen, X.J. Jiao, J. Phys. Chem. C 113 (2009) 7714–7718.
[38] D. Larcher, R. Sudant, R. Patrice, J.M. Tarascon, Chem. Mater. 15 (2003) 3543–3551.
[39] X.C. Jiang, Y.L. Wang, T. Herricks, Y.N. Xia, J. Mater. Chem. 14 (2004) 695–703.
[40] Z.Y. Tang, J.H. Wu, M. Zheng, Q.W. Tang, Q. Liu, J.M. Lin, J.L. Wang, RSC Adv. 2 (2012) 4062–4064.
[41] T.W. Hamann, R.A. Jensen, A.B.F. Martinson, H.V. Ryswykac, J.T. Hupp, Energy Environ. Sci. 1 (2008) 66–78.
[42] G.L. Zhang, K. Pan, W. Zhou, Y. Qu, Q.J. Pan, B.J. Jiang, G.H. Tian, G.F. Wang, Y. Xie, Y.Z. Dong, X.H. Miao, C.G. Tian, Dalton Trans. 41 (2012) 12683–12689.
[43] L.-H. Chang, C.-K. Hsieh, M.-C. Hsiao, J.-C. Chiang, P.-I. Liu, K.-K. Ho, C.-C.M. Ma, M.-Y. Yen, M.-C. Tsai, C.-H. Tsai, J. Power Sources 222 (2013) 518–525.